

Fully superconducting machine for electric aircraft propulsion: study of AC loss for HTS stator

Fangjing Weng , Min Zhang , Tian Lan, Yawei Wang  and Weijia Yuan

Department of Electronic and Electrical Engineering, University of Strathclyde, G1 1XQ Glasgow, United Kingdom

E-mail: min.zhang@strath.ac.uk and wengfangjing@vip.163.com

Received 3 December 2019, revised 28 April 2020

Accepted for publication 26 May 2020

Published 18 August 2020



Abstract

Fully superconducting machines provide the high power density required for future electric aircraft propulsion. However, superconducting windings generate AC losses in AC electrical machine environments. These AC losses are difficult to eliminate at low temperatures, and they add an extra burden to the aircraft cooling system. Due to the heavy cooling penalty, AC loss in the HTS stator is one of the key topics in HTS machine design. In order to evaluate the AC loss of superconducting stator windings in a rotational machine environment, we designed and built a novel axial-flux high temperature superconducting (HTS) machine platform. The AC loss measurement is based on the calorimetric boiling-off of liquid nitrogen. Both total AC loss and magnetisation loss in the HTS stator are measured under the condition of a rotational magnetic field. This platform represents a key element in studying ways to minimise AC losses in an HTS stator, in order to maximise the efficiency of fully HTS machines.

Keywords: 2G HTS, fully HTS machine, AC loss, calorimetric method, electric aircraft

(Some figures may appear in colour only in the online journal)

1. Introduction

The power density of current electrical machines is not high enough for advanced propulsion applications in all electric aircraft [1–12]. Compared to conventional machines with copper windings, superconducting machines can significantly reduce machine volume and weight, thereby significantly increasing power density. The latest high temperature superconductors (HTS) exhibit high critical currents at relatively high operational temperatures, which can significantly increase the machine power density. Partially HTS machines, based on HTS rotors and copper stators, have been developed [13, 14]. However, previous cold-rotor-warm-stator designs led to large air gaps, thereby reducing the magnetic field. To fully utilize

the advantages of HTS windings, fully HTS machines have been proposed, in order to maximize machine power density for applications [10, 15, 16].

In a fully HTS machine, the HTS stator is subjected to a rotational AC magnetic field, as well as an AC transport current. This generates AC losses, which potentially increases the size and weight of the machine cooling system. The key challenge of developing a fully HTS machine is to minimise HTS winding AC losses. So far, most of the research in the area of HTS tapes and coils has focused on transport AC loss or magnetisation loss in a uniform magnetic field [17–28]. Few studies have dealt with the issue of the AC loss of HTS in a rotational magnetic field [29]. The US Air force proposed the measurement of magnetisation loss in a rotational magnetic field generated by a radial type permanent magnet rotor. However, their study does not consider the influence of transport currents [10].

Previous studies including an AC background magnetic field have been conducted on the subject of the calorimetric



Original content from this work may be used under the terms of the [Creative Commons Attribution 4.0 licence](https://creativecommons.org/licenses/by/4.0/). Any further distribution of this work must maintain attribution to the author(s) and the title of the work, journal citation and DOI.

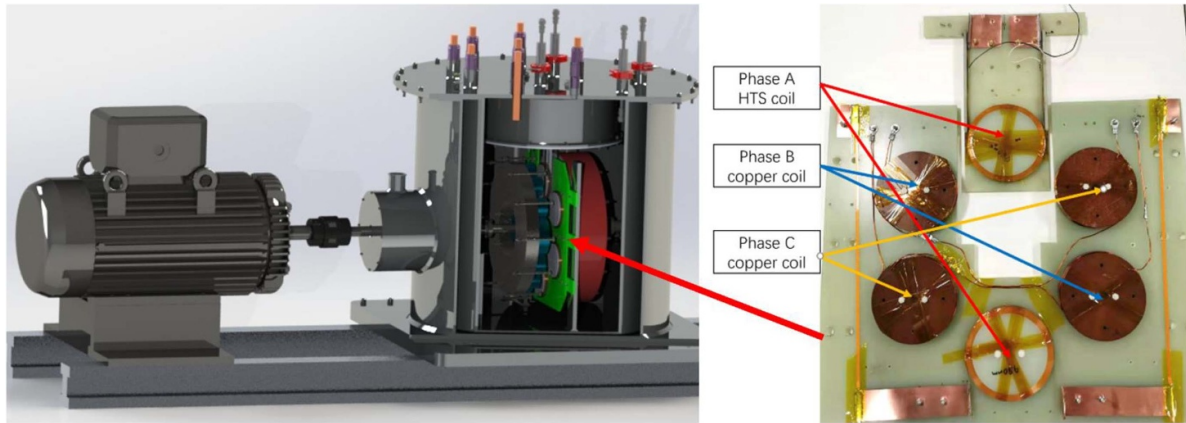


Figure 1. Structure of the measurement chamber.

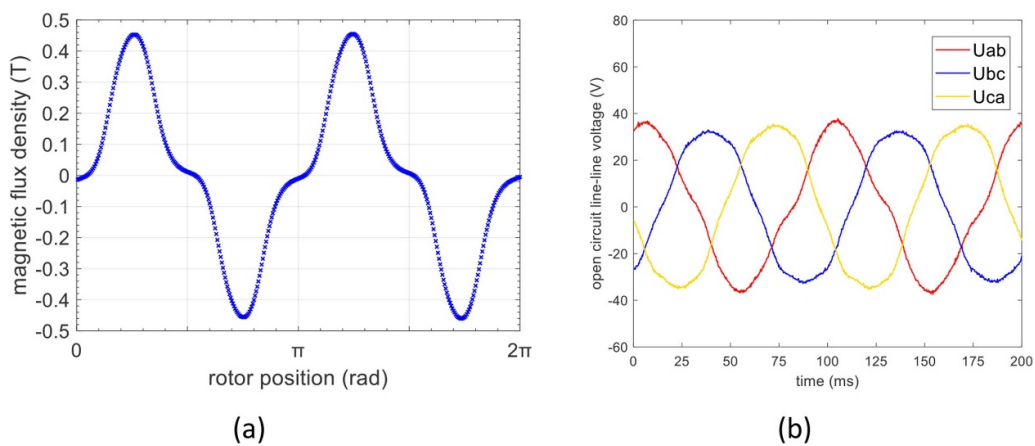


Figure 2. (a) Measured magnetic flux field distribution; (b) 3-phase line-line voltages.

method for AC loss measurement of HTS at liquid nitrogen temperature (77 K), [10, 30–33], by measuring the boil-off rate of LN₂. The main advantage of using the calorimetric method is that it can measure the total loss from an HTS coil, regardless of the phase difference between the applied current and the background field [34, 35]. There is a lack of measurement systems to study AC loss in rotational machines. In this paper, a novel HTS machine platform is proposed, based on the calorimetric method, in order to measure the total AC loss in a rotational magnetic field. Section 2 demonstrates the whole system design and setup, section 3 explains system calibration and validation, section 4 illustrates the AC loss measurement results, and section 5 discusses the results and conclusions.

2. The axial-flux HTS machine platform design

2.1. Machine design

In order to enable the LN₂ boil off measurement inside a rotational machine, we have chosen the axial-flux machine design, so as to accommodate a measurement chamber for an HTS stator winding, as shown in figure 1. This machine contains two four-pole permanent magnet rotor discs, two silicon steel

back irons and a three-phase HTS stator. Each rotor disc consists of four large NdFeB permanent magnets, each with a diameter of 100 mm, sitting on a laminated silicon steel plate. The HTS stator disc is sandwiched between two rotor discs, and consists of six stator coils. Only two coils of phase A are constructed of HTS materials, as shown in figure 4; phase B and phase C are constructed of copper coils with the same diameter. The measurement coil was placed in a separate measurement chamber with liquid nitrogen.

The machine is hosted in a LN₂ cryostat with a rotational seal. Due to the limitations of the bearings, this machine is designed to operate at a speed of 300 RPM, generating a 10 Hz three-phase voltage output. A hall sensor was placed across the air-gap in order to measure the magnetic field in the coil center; a peak magnetic flux density of 0.45 T was measured in the center, as shown in figure 2(a). The phase A voltage was generated by two HTS coils, while the voltages of phase B and C were generated by copper coils. The peak voltage of the HTS is slightly higher, due to the inductance difference between HTS materials and copper (copper coil inductance = 526.4 μ H, whereas HTS coil inductance = 937.4 μ H). Analysis of the spectrum of each phase voltage via FFT calculation reveals that only the 3rd harmonic with a small amplitude occurs in the stator windings, due to the magnetic field distribution, as

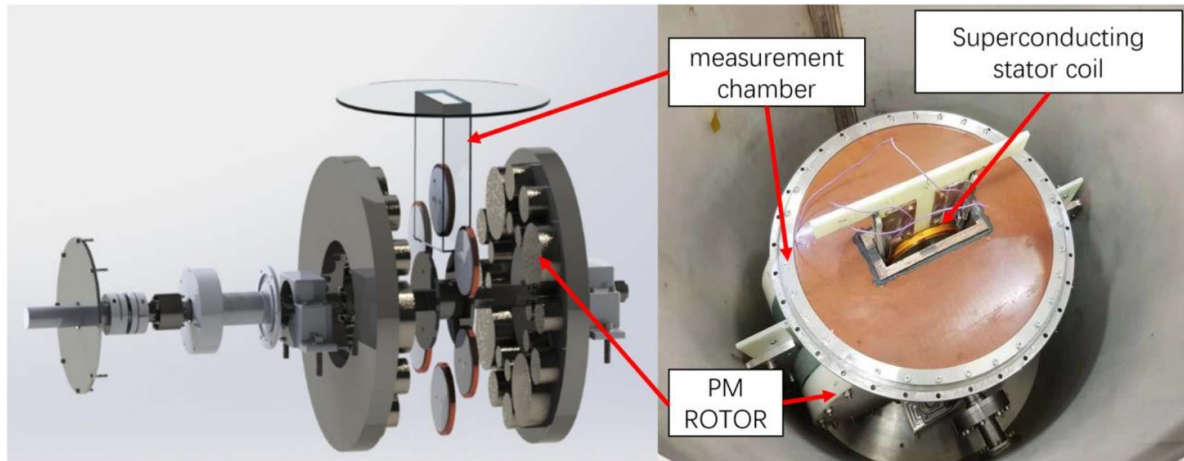


Figure 3. Measurement chamber configuration.

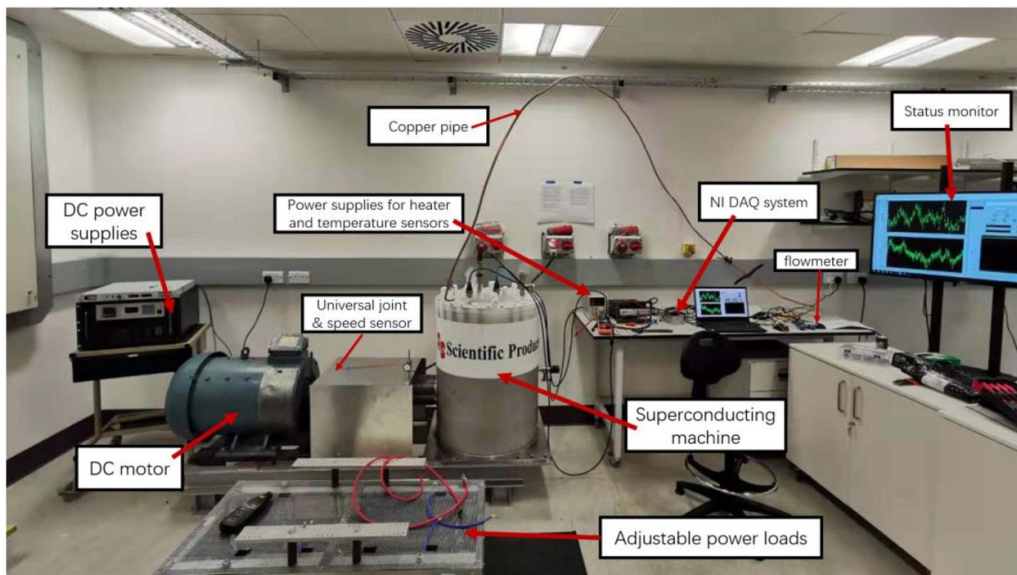


Figure 4. Total HTS machine system configuration.

well as the non-linear performance of the silicon steel. The 3rd harmonic may be eliminated via star-connection; thus this machine achieves a good sinusoidal voltage, as shown in figure 2(b).

2.2. Cryostat design

In order to measure the boil-off rate of liquid nitrogen generated by the total AC loss of HTS stator coils, a dedicated measurement chamber was designed, as illustrated in figure 3. Only one HTS stator coil is placed in the measurement chamber. It is connected to a flow meter to measure the flow rate of the nitrogen gas. The measurement chamber is fully immersed in LN₂ to minimise heat transfer; both rotor and stator are fully immersed in liquid nitrogen during operation. Under ideal conditions, there should be no heat transfer between the two chambers. The only conducting component inside the measurement chamber is the HTS stator coil, which ensures that the boil-off

of liquid nitrogen is due only to the total AC loss of the HTS coil.

The nitrogen gas flow rate is measured by a flow meter (Omega FMA 2710). Theoretically, the latent heat for liquid nitrogen is 160.6 J ml⁻¹ [36], which is equal to 0.25 standard litre per minute for every Watt of power (SLPM/W). Total AC loss of T can be calculated using equation (1) [19].

$$Q = \int_T \frac{F(t)}{K} dt \quad (1)$$

where Q (Joule) is the total heat produced in the measurement chamber for a duration of T , and $F(t)$ is the flow rate of nitrogen gas boiled off in the measurement chamber measured by a flow meter. $K = 0.256$ (l min⁻¹ W⁻¹) is the flow rate constant. When the HTS machine operates in steady state with a fixed frequency f , $F(t)$ in equation (1) is simply a constant value with a very small fluctuation; subsequent to calibration procedures, we can calculate coil AC loss accordingly. By measuring the

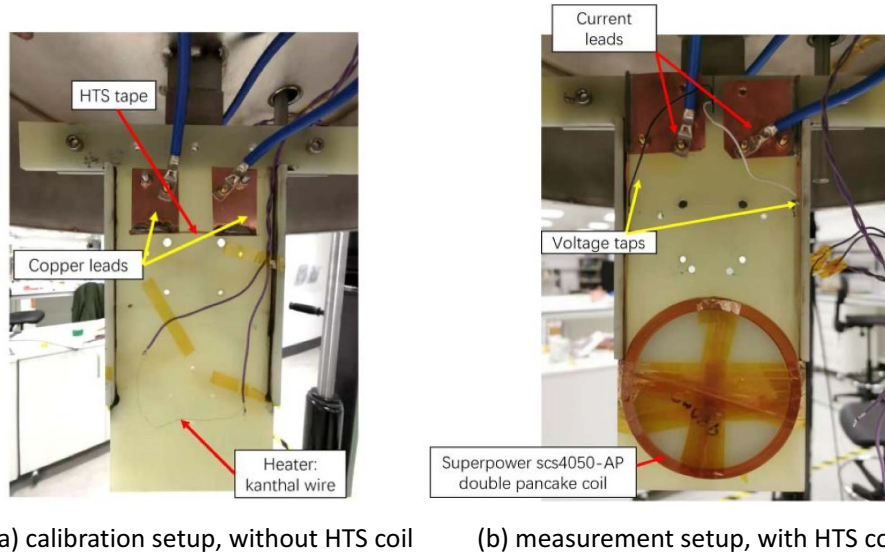


Figure 5. Setup in measurement chamber. (a) Calibration setup, without HTS coil, (b) measurement setup, with HTS coil.

nitrogen gas flow rate, and calibrating the value of the AC loss element, AC loss can then be calculated.

2.3. System setup

The entire system setup is illustrated in figure 4. The separately excited DC motor is driven by 2 DC power supplies; during the measurement procedure, the rotation of the HTS rotors is driven by a DC machine. The HTS stator coil is connected to a load bank, generating three-phase electricity. The LN2 level in the cryostat is observed by 4 PT100 temperature sensors, LN2 boil-off flow rate is recorded by a flow meter, and all data were recorded by a NI DAQ system. An overview of the HTS machine performance, including coil voltages, coil currents, motor speed, flow meter data, and LN2 level, is recorded by a status monitor.

3. System calibration and validation

Based on the above platform setup, total heat input to the measurement chamber consists of the following elements in equation (2):

$$Q_{total} = Q_{HTS} + Q_{background} + Q_{rotation} + Q_{terminal} \quad (2)$$

Q_{total} refers to the total heat produced in the chamber, Q_{HTS} refers to the heat caused by the HTS coil AC loss, $Q_{background}$ refers to the unavoidable heat leakage in the system, $Q_{rotation}$ refers to the thermal balance condition change when liquid nitrogen was stirred by the rotor, and to the Joule heat produced by other stator coils, and $Q_{terminal}$ refers to the Joule heat caused by copper terminal and solder joint resistance between HTS and copper current leads. These losses in equation (2) can be quantified by a set of calibration procedures.

For the calibration procedures, the HTS coil in the measurement chamber was replaced by a very short HTS tape between

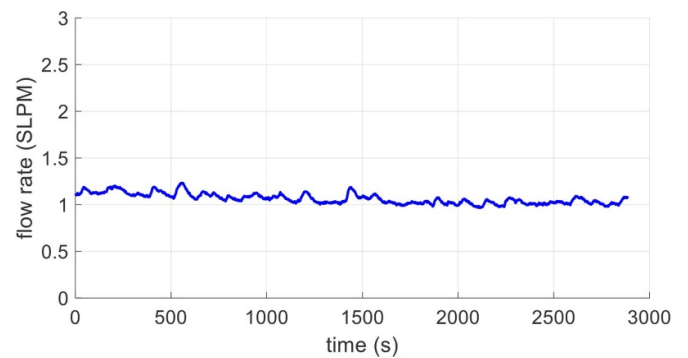


Figure 6. Background flow rate data.

two copper terminals, and one heater made of Kanthal resistance wire (26.4 ohms) was placed in the system, as shown in figure 5(a). Figure 5(b) demonstrates the normal measurement setup with an HTS coil.

3.1. $Q_{background}$ measurement

Prior to the onset of calibration, both the measurement chamber and the outer cryostat were filled with liquid nitrogen, ensuring that the system was cooled to 77 K. The flow meter (Omega FMA 2710) was connected to the measurement chamber via a long copper pipe. A background flowrate (referred to as $Q_{background}$ in equation (3)) was measured when the rotor was static, over a period of 3000 s, and the results of the flow meter, as shown in figure 6, give a background flowrate of 1.1 SLPM. According to equation (1), the background heat power measurement is 4.29 W, due to heat leakage and environmental radiation.

Figure 6 illustrates that background flow rate can be regarded as a constant value for a short time. $Q_{background}$ can be calibrated by subtracting the background flow rate.

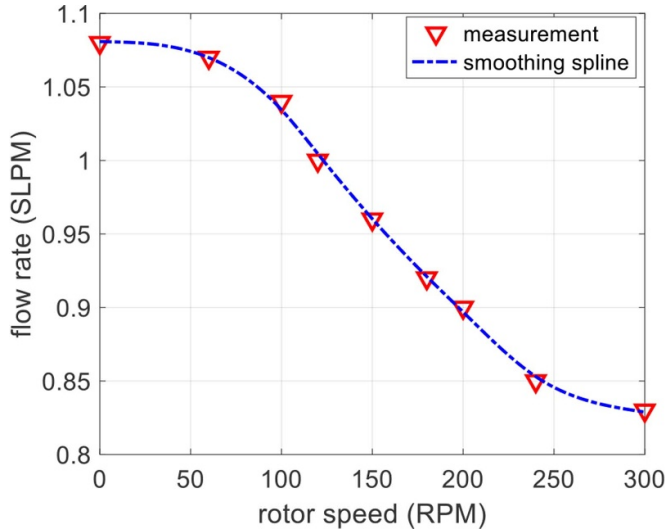


Figure 7. Rotor speed calibration.

3.2. $Q_{terminal}$ calibration

As shown in figure 5(b), two terminals of the HTS coil were soldered to two copper current leads, then connected to two copper bars fed through the top flange; therefore, resistance will be present in the copper bars and copper current leads, and there will also be a contact resistance in the solders between the HTS tape and the copper current leads. When a transport current occurs, we obtain $Q_{terminal}$. The impact of terminal resistance can be measured by shorting two copper terminals. For this measurement, the HTS coil was replaced by a short HTS tape, as shown in figure 5(a). A 6 cm HTS tape was soldered between two copper current leads. A DC power supply was then connected from the outside, providing a current from 0–80 A. According to equation (1), the heat power (W) can be expressed by equation (3):

$$I^2 R_{terminal} = \frac{\Delta F}{K} \quad (3)$$

where I is a constant DC current, $R_{terminal}$ is the terminal resistance, ΔF refers to a calibrated flow rate (subtracting the $Q_{background}$ flow rate 1.1 SLPM from the total flow rate), and K is the flowrate constant ($0.256 \text{ SLPM W}^{-1}$ in our setup). Thus, a terminal resistance of $0.243 \text{ m}\Omega$ was calculated, which requires to be calibrated out by means of equation (4):

$$Q_{terminal} = 2.43 \times 10^{-4} I^2 t \quad (4)$$

where $Q_{terminal}$ denotes the Joule heat by terminal resistance for a duration of t , and I is the transport current.

3.3. $Q_{rotation}$ calibration

When the HTS machine is fully operational, the rotor speed is 300 RPM; in addition, there is also 40 A peak current in the stator. The rotation of the rotors will stir the liquid nitrogen in the outer cryostat, thereby altering the heat transfer balance; this may cause the flow rate to change in the measurement

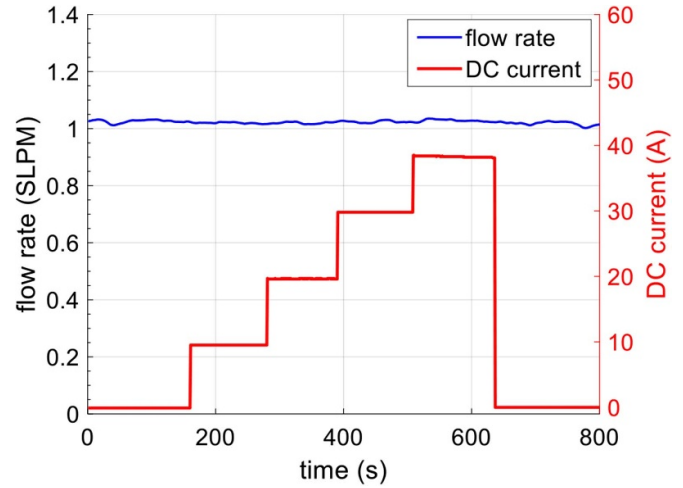


Figure 8. Stator coils current calibration.

chamber. As for the stator, since phase B and phase C consist of copper coils, the current will generate Joule heat. Although the measurement chamber is made of Tufnol, which is good thermal isolation material, some heat may still transfer to the inner cryostat, causing a flow rate change.

The rotor speed calibration took place with open-circuit stator windings, thus there was no current in the stator. The rotor speed was measured between 0 to 300 RPM, and each speed was maintained for more than 20 min. A fluctuation level lower than 0.08 SLPM was observed, based on the nine recorded data shown in figure 8. When the speed increased from 0 to 300 RPM, flow rate decreased from 1.07 SLPM to 0.83 SLPM. Heat transfer was balanced when the rotor speed was steady; when the liquid nitrogen was stirred by the rotor, some liquid nitrogen cooling of the top plate and the foams occurred, causing the system to proceed to a new thermal balance condition. With an increase in the rotor speed, the temperature difference between the measuring chamber and the top plate decreased, resulting in a lower background flow rate. Thus, any error caused by rotor speed could be calibrated out as illustrated in figure 7.

The stator is designed to operate at a peak current of 40 A; thus, stator calibration is achieved simply by keeping the rotor static, with no input power to the inner cryostat. Current was applied to all five stator coils in the outer cryostat, and flow meter data was recorded. The results are shown in figure 8, where the red curve illustrates the DC current applied to the stator, and the blue line denotes the flow rate during this time. As we can see from the results, flow rate does not change when different currents are applied to the stator. Figure 8 demonstrates the good thermal isolation of the Tufnol material, and that the heat transfer value is very small, implying that the stator's Joule heat has no influence on the flow rate. Thus, $Q_{rotation}$ is caused only by the rotor speed, and can be calibrated out via the method shown in figure 7.

3.4. Measurement chamber calibration

Theoretically, the flow rate constant should equal 0.25 standard litre per min per watt (SLPM W^{-1}). A resistance wire of

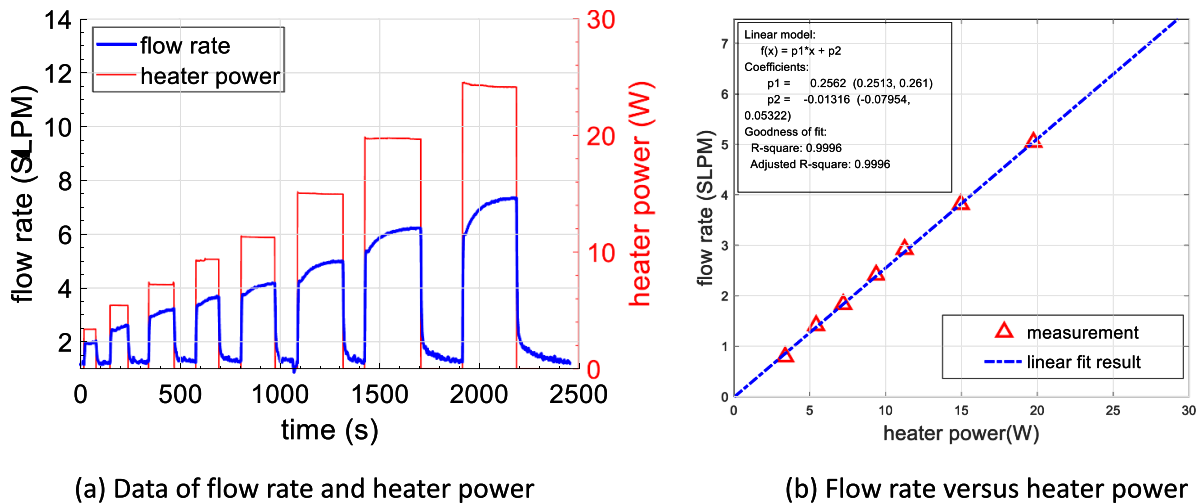


Figure 9. Background flow rate data. (a) Data of flow rate and heater power, (b) flow rate versus heater power.

Table 1. Specification of HTS stator winding coil.

Parameters	Value
Tape type	Superpower SCS4050-AP
Tape I_c	140 A
Coil I_c (self-field)	72 A
Coil inner diameter	95 mm
Coil outer diameter	99.8 mm
Turns per layer	38
Total coil turns	76
Inductance	937.4 μH

26.4 ohms (in liquid nitrogen) was placed in the measurement chamber, and connected to a DC power source. During the heater calibration procedure, various DC voltages from 0–25.2 V were applied, and eight points were selected, from 3.38 W to 24.16 W. Figure 9(a) demonstrated the results of flow rate (subtracting the background flow) induced by various heating powers applied to the resistance wire. The red curve denotes the heater power level, and the blue curve indicates the flow rate after calibration. These data are then plotted in one figure, as illustrated in figure 9(b). The results show the flow rate proportional to heating power in the measurement chamber, the curve giving a ratio of 0.256 SLPM W^{-1} refers to the flow rate constant. These experimental results show that the actual performance is in accordance with the theoretical value, with an error value of only 2.4%. On the other hand, figure 9 validates the system, demonstrating that there was no gas leakage in the measurement chamber, as the range of fluctuation of the flow meter is less than 0.08 SLPM, which gives a measuring error of up to 0.3 W.

To sum up: all errors have been estimated and well calibrated, and the sensitivity of this testing rig has a value near to 0.3 W, commensurate with a platform based on the calorimetric method.

4. AC loss of a HTS stator

The HTS coil is prepared using 25 m of 4 mm superpower SCS 4050-AP tape. The single tape critical current is 140 A.

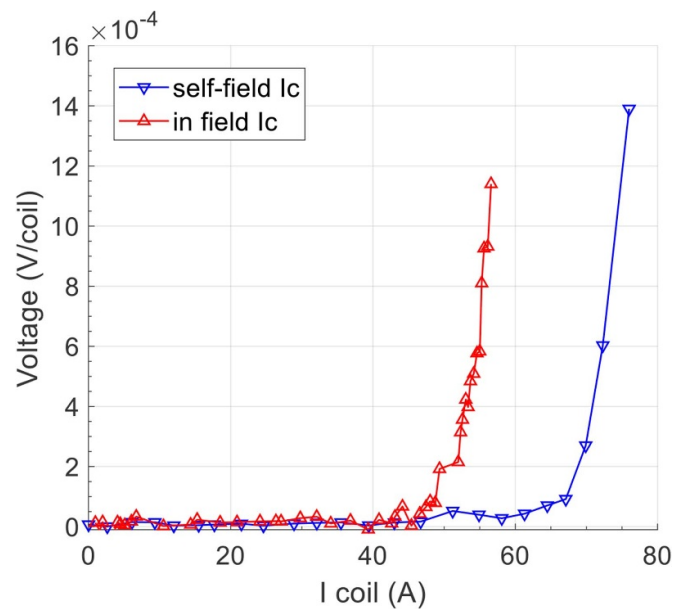


Figure 10. Self-field and in-field critical current.

The specification of the HTS double pancake coil is shown in table 1, and an image of the coil and setup is shown in figure 5(b).

Both self-field coil critical current and in-field critical current were measured, and the results were as shown in figure 10; by using $0.1 \mu\text{V cm}^{-1}$ criteria, the self-field critical current measures 72 A, and the in-field critical current measures 53 A (at peak 0.45 T). Thus, this coil operates satisfactorily at a peak current of 40 A.

4.1. Magnetisation loss

The magnetisation loss of this coil can be measured by keeping the HTS coil open circuited, so that there is no transport current in the HTS coil, and only the magnetisation loss is measured. We measured five different frequencies (3.33 Hz, 5.00 Hz, 6.67 Hz, 8 Hz, and 10 Hz); as this is a two-pole-pair

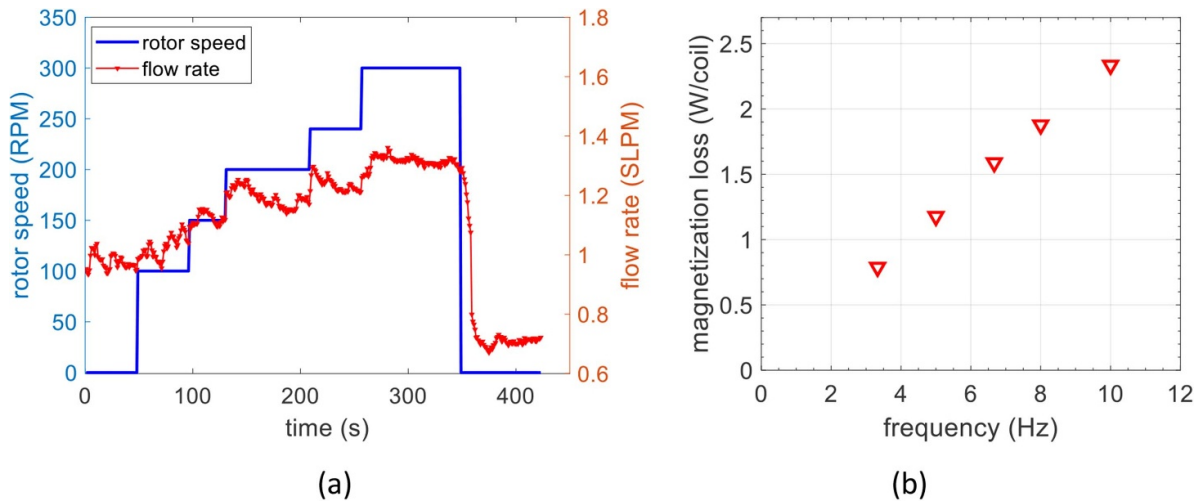


Figure 11. Magnetisation loss versus frequency.

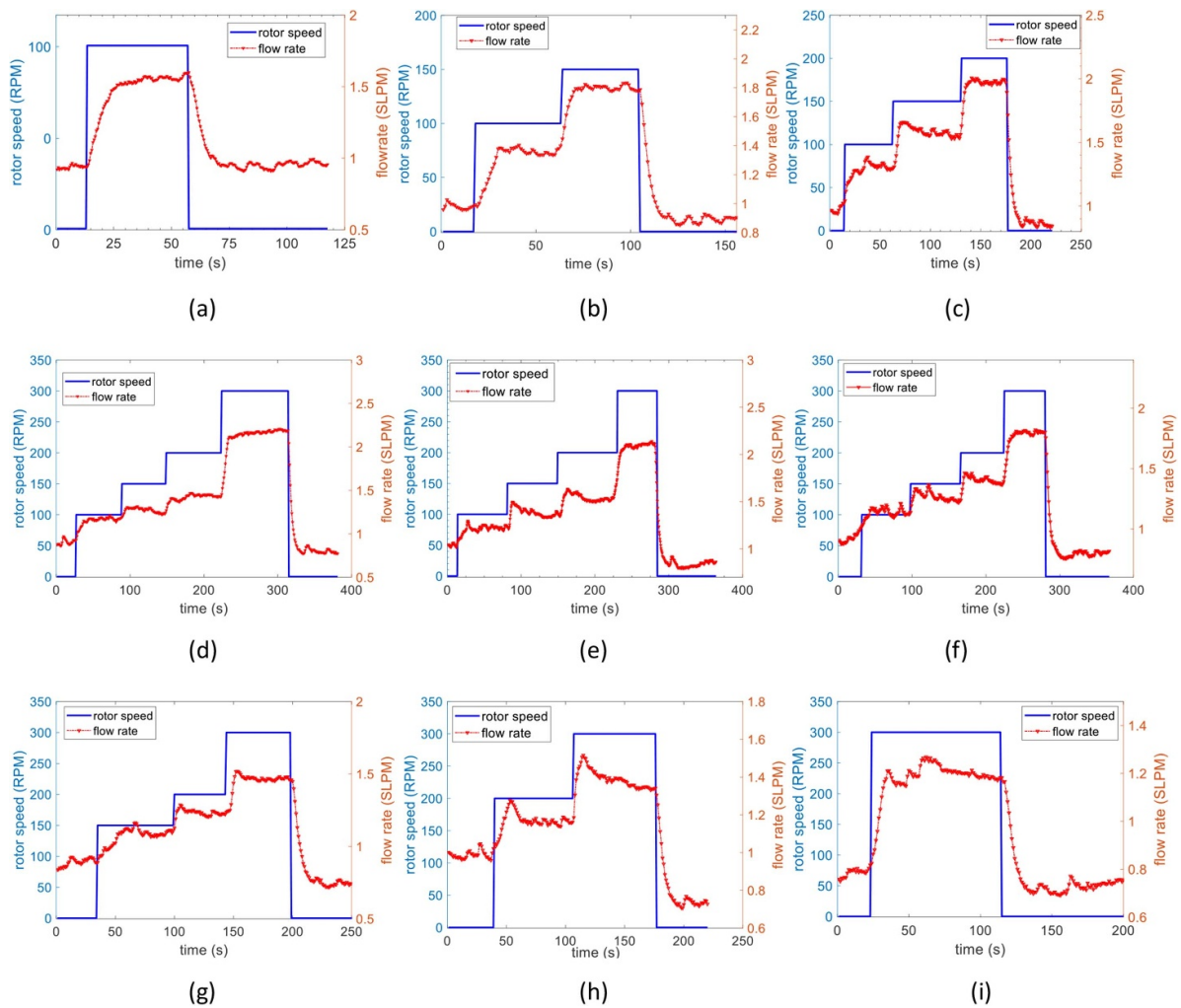


Figure 12. Total AC loss measurements.

rotor, these frequencies correspond to rotor speeds of 100, 150, 200, 240, and 300 RPM, respectively. The results of the flow rate data recorded at these frequencies (the sample rate of data acquisition is 20 S s^{-1}) are shown in figure 11(a), where the

red line indicates flow rate data, and the blue line denotes the rotor speed. When the rotor speed increases, the thermal equilibrium condition changes to a new thermal balance condition. After a short period of thermal imbalance, a fluctuation level

Table 2. Transport current values in figure 12.

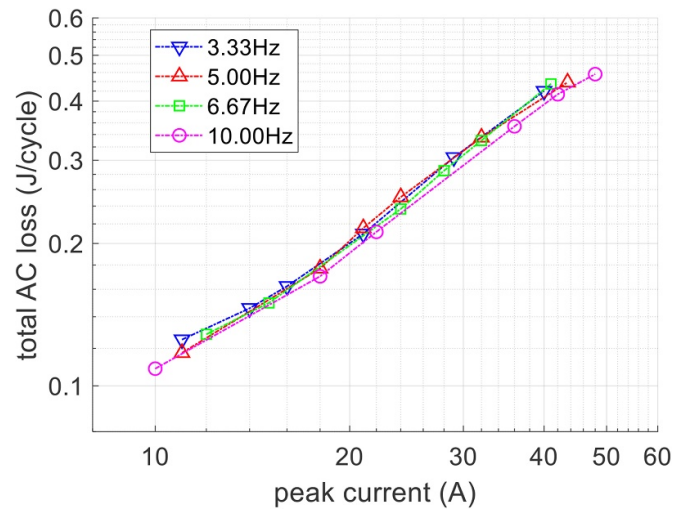
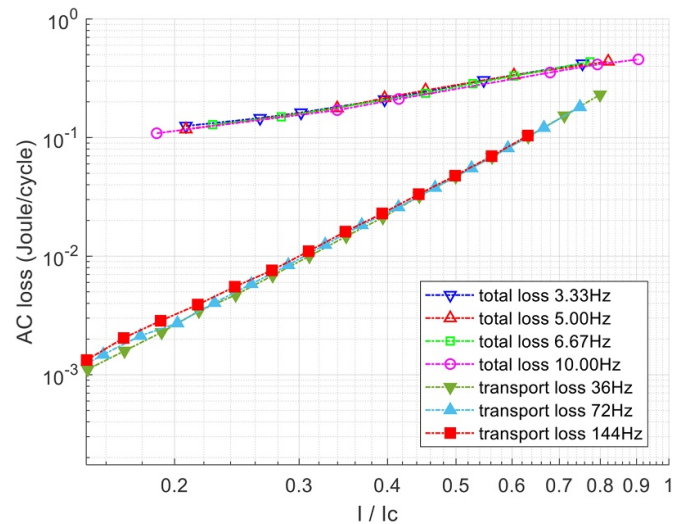
	3.33 Hz	5.00 Hz	6.67 Hz	10.00 Hz
Figure 12(a)	40 A			
(b)	29 A	43.5 A		
(c)	21 A	32 A	41 A	
(d)	16 A	24 A	32 A	48 A
(e)	14 A	21 A	28 A	42 A
(f)	11 A	18 A	24 A	36 A
(g)		11 A	15 A	22 A
(h)			12 A	18 A
(i)				10 A

lower than 0.08 SLPM was observed. These fluctuations are caused by small bubbles of nitrogen gas in the measurement chamber; thus, an integral operation may be used to calculate the total nitrogen gas volume for the previous 10 s. Subsequent to calibrating out flow-rate errors via equation (3), the magnetisation loss of this coil versus frequency can then be calculated by means of equation (2), as shown in figure 12(b).

In order to estimate the magnetisation loss, finite element modeling is used for magnetisation loss calculation. Previous studies have demonstrated that finite element modeling using H-formulation can estimate AC loss for a double pancake coil. Our double pancake coil specification is shown in table 1. A COMSOL modeling of this coil was developed using a 2D axis-symmetric model, and H-formulation[37]. We simplify the model via the application of a time-variant magnetic field using figure 2(a), and the FEM simulation results indicated at 10 Hz, giving a magnetisation loss for the double pancake coil of 2.2 W. As this value is calculated by means of a time-variant magnetic field waveform, the magnetic environment is not exactly the same as for the experiments. Thus, the simulation result can only be used to estimate the magnetisation loss level.

4.2. Total AC loss

The total AC loss of the single HTS coil is measured by connecting the three-phase stator windings to adjustable power resistors. To measure the total AC loss with various currents, the resistors must be changed. We measured six different peak transport currents between 10 A and 40 A for four frequencies (3.33 Hz, 5 Hz, 6.67 Hz, and 10 Hz), corresponding to rotor speeds at 100, 150, 200, and 300 RPM, respectively. Flow rate data from the experiments are illustrated in figure 12, where the blue curves refer to the rotor speed, and the red curves refer to the instantaneous flow rate value. The transport current values for different frequencies are shown in table 2. The AC loss is a small value when a small transport current, is applied and also at low frequencies. If the level of fluctuation falls below 0.08 SLPM for more than 1 min, an integral operation may be used to calculate the flow rate data for the previous 10 s, in order to improve accuracy. Having calibrated out the errors via equation (3), the total AC loss versus transport current is shown in figure 13. Figure 14 shows a comparison between the total AC loss and the transport AC loss. The results show that

**Figure 13.** Measured total AC loss.**Figure 14.** Transport loss and total loss.

a rotational field of 0.45 T significantly increases the AC loss of the coil.

Our results show that at a peak current of 73% I_c and a peak rotational field of 0.45 T, the HTS coil generates a total of 4.56 W of heat at 10 Hz and 48 A. To further understand the impact of a rotational magnetic field, we compared the transport loss of the HTS coil with the total AC loss, as shown in figure 14. The transport loss was measured at 77 K using the four-point electrical method [19, 38]. The total AC loss is very high for standard 4 mm HTS conduction used as machine windings. To minimize the total AC losses from HTS stator windings, new HTS winding solutions to reduce AC loss are essential. One advantage of this platform is that it enables a comparison of the AC loss for different HTS windings. For example, we plan to measure a 1 mm wide multi-filament HTS cable coil with the same geometry as the HTS coil used in this paper, and to quantify its loss reduction in a machine environment [39, 40].

5. Conclusion and future work

The platform is verified and validated for AC loss measurements, but uncertainties do not create a significant percentage error, and, as can be observed the total error level is less than 0.3 W (0.08 SLPM). The results are more accurate with the application of higher current and at higher frequencies, as HTS machine applications are normally required to carry a high current (near its critical current value); thus, this platform can provide experimental results for machine design.




The measurement of total AC losses in figure 13 was performed in a generator mode, so the transport current and the rotational magnetic field are in phase. As demonstrated in our previous work, the phase angle between the transport current and the external magnetic field affects total AC losses [6]. When the current and magnetic field are in phase, the total AC loss is the highest. Our next step will be to use a machine drive to operate the machine in a motor operational mode, so as to control the phase angle and measure its impact in relation to total AC losses. There is also the possibility of testing the impact of powered electronic devices to the AC losses of an HTS stator by connecting them together and measuring the AC losses.

This paper demonstrates a pioneering testing platform for fully HTS machines, to be used for future electric aircraft machines. The system was carefully calibrated and validated, and provides a machine environment to measure the AC loss of HTS windings. Focusing on the calorimetric quantification of an electrical HTS stator, this platform can provide valuable insights into the AC losses of HTS stators in a rotational machine environment. The platform can also be used for the identification of AC loss reduction technologies, contributing to the development of a highly efficient fully HTS propulsion machine.

Acknowledgments

This project is funded by Royal Academy Research Fellowship, under the project 'Fully superconducting machines for next generation electric aircraft propulsion', and the EPSRC Grant EP/P002277/1 'Developing Highly efficient HTS AC windings for fully superconducting machines'. Fangjing Weng would like to acknowledge the support of the Chinese Scholar Council Grant #201908060381. The authors would also like to thank Dr Jay Patel for his contribution in preparing figures 1 and 3.

ORCID iDs

Fangjing Weng  <https://orcid.org/0000-0003-4008-976X>
 Min Zhang  <https://orcid.org/0000-0003-4296-7730>
 Yawei Wang  <https://orcid.org/0000-0003-2390-2835>

References

- [1] Luongo C A, Masson P J, Nam T, Mavris D, Kim H D, Brown G V, Waters M and Hall D 2009 Next generation

- more-electric aircraft: a potential application for HTS superconductors *IEEE Trans. Appl. Supercond.* **19** 1055–68
- [2] Armstrong M J, Ross C A, Blackwelder M J and Rajashekara K 2012 Propulsion system component considerations for NASA N3-X turboelectric distributed propulsion system *SAE Int. J. Aerosp.* **5** 344–53
- [3] Sarlioglu B and Morris C T 2015 More electric aircraft: review, challenges, and opportunities for commercial transport aircraft *IEEE Trans. Transp. Electrification* **1** 54–64
- [4] Bertola L, Cox T, Wheeler P, Garvey S and Morvan H 2016 Superconducting electromagnetic launch system for civil aircraft *IEEE Trans. Appl. Supercond.* **26** 3602911
- [5] Berg F, Palmer J, Miller P, Husband M and Dodds G 2015 HTS electrical system for a distributed propulsion aircraft *IEEE Trans. Appl. Supercond.* **25** 1–5
- [6] Brown G 2011 Weights and efficiencies of electric components of a turboelectric aircraft propulsion system *49th AIAA aerospace sciences meeting including the new horizons forum and aerospace exposition* p 225
- [7] Gohardani A S, Douglgeris G and Singh R 2011 Challenges of future aircraft propulsion: a review of distributed propulsion technology and its potential application for the all electric commercial aircraft *Prog. Aerosp. Sci.* **47** 369–91
- [8] Henke M, Narjes G, Hoffmann J, Wohlers C, Urbanek S, Heister C, Steinbrink J, Canders W R and Ponick B 2018 Challenges and opportunities of very light high-performance electric drives for aviation *Energies* **11** 344
- [9] Vepa R 2018 Modeling and dynamics of HTS motors for aircraft electric propulsion *Aerospace* **5** 21
- [10] Zhang M, Yuan W, Kvitkovic J and Pamidi S 2015 Total AC loss study of 2G HTS coils for fully HTS machine applications *Supercond. Sci. Technol.* **28** 115011
- [11] Ainslie M, Izumi M and Miki M 2016 Recent advances in superconducting rotating machines: an introduction to the 'focus on superconducting rotating machines' *Supercond. Sci. Technol.* **29** 060303
- [12] Song P, Qu T, Lai L, Wu M, Yu X and Han Z 2016 Thermal analysis for the HTS stator consisting of HTS armature windings and an iron core for a 2.5 kW HTS generator *Supercond. Sci. Technol.* **29** 054007
- [13] Eckels P and Snitchler G 2005 5 MW high temperature superconductor ship propulsion motor design and test results *Nav. Eng. J.* **117** 31–36
- [14] Nick W, Grundmann J and Frauenhofer J 2012 Test results from Siemens low-speed, high-torque HTS machine and description of further steps towards commercialisation of HTS machines *Physica C* **482** 105–10
- [15] Li S, Fan Y, Fang J, Qin W, Lv G and Li J 2013 HTS axial flux induction motor with analytic and FEA modeling *Physica C* **494** 230–4
- [16] Qu T, Song P, Yu X, Gu C, Li L, Li X, Wang D, Hu B, Chen D and Zeng P 2014 Development and testing of a 2.5 kW synchronous generator with a high temperature superconducting stator and permanent magnet rotor *Supercond. Sci. Technol.* **27** 044026
- [17] Wang Y, Song H, Yuan W, Jin Z and Hong Z 2017 Ramping turn-to-turn loss and magnetization loss of a no-insulation (RE) $\text{Ba}_2\text{Cu}_3\text{O}_x$ high temperature superconductor pancake coil *J. Phys. D: Appl. Phys.* **121** 113903
- [18] Wang Y, Guan X and Dai J 2014 Review of AC loss measuring methods for HTS tape and unit *IEEE Trans. Appl. Supercond.* **24** 1–6
- [19] Kim J-H, Kim C H, Iyyani G, Kvitkovic J and Pamidi S 2011 Transport AC loss measurements in superconducting coils *IEEE Trans. Appl. Supercond.* **21** 3269–72
- [20] Gömöry F, Vojenčiak M, Pardo E, Solovyov M and Šouc J 2010 AC losses in coated conductors *Supercond. Sci. Technol.* **23** 034012

- [21] Šouc J, Pardo E, Vojenčiak M and Gömöry F 2008 Theoretical and experimental study of AC loss in high temperature superconductor single pancake coils *Supercond. Sci. Technol.* **22** 015006
- [22] Grilli F and Ashworth S P 2007 Measuring transport AC losses in YBCO-coated conductor coils *Supercond. Sci. Technol.* **20** 794
- [23] Wang Y, Zhang M, Grilli F, Zhu Z and Yuan W 2019 Study of the magnetization loss of CORC® cables using a 3D T-A formulation *Supercond. Sci. Technol.* **32** 025003
- [24] Pei X, Smith A C, Zeng X, Husband M and Rindfleisch M 2013 Design, build and test of an AC coil using MgB₂ wire for use in a superconducting machine *IEEE Trans. Appl. Supercond.* **23** 5202605–
- [25] Yang Y, Martinez E and Norris W 2004 Configuration and calibration of pickup coils for measurement of ac loss in long superconductors *J. Phys. D: Appl. Phys.* **96** 2141–9
- [26] Majoros M, Sumption M, Susner M, Collings E, Souc J, Gomory F, Vojenciak M, Fisher L, Kalinov A and Voloshin I 2011 AC magnetization loss of a YBCO coated conductor measured using three different techniques *IEEE Trans. Appl. Supercond.* **21** 3293–6
- [27] Hong Z, Yuan W, Ainslie M, Yan Y, Pei R and Coombs T 2010 AC losses of superconducting racetrack coil in various magnetic conditions *IEEE Trans. Appl. Supercond.* **21** 2466–9
- [28] Brandt E H and Indenbom M 1993 Type-II-superconductor strip with current in a perpendicular magnetic field *Phys. Rev. B* **48** 12893
- [29] Zhang M, Wang W, Huang Z, Baghdadi M, Yuan W, Kvitkovic J, Pamidi S and Coombs T 2014 AC loss measurements for 2G HTS racetrack coils with heat-shrink tube insulation *IEEE Trans. Appl. Supercond.* **24** 1–4
- [30] Carr W 1979 AC loss from the combined action of transport current and applied field *IEEE Trans. Magn.* **15** 240–3
- [31] Ashworth S and Suenaga M 1999 The calorimetric measurement of losses in HTS tapes due to ac magnetic fields and transport currents *Physica C* **315** 79–84
- [32] Hardono T, Cook C D and Jin J-X 1999 Measurements of AC losses in HTSC wires exposed to an alternating field using calorimetric methods *IEEE Trans. Appl. Supercond.* **9** 813–6
- [33] Daney D, Boenig H, Maley M, McMurry D and DeBlanc B 1997 AC loss calorimeter for three-phase cable *IEEE Trans. Appl. Supercond.* **7** 310–3
- [34] Pardo E 2013 Calculation of AC loss in coated conductor coils with a large number of turns *Supercond. Sci. Technol.* **26** 105017
- [35] Šouc J, Gömöry F and Vojenčiak M 2005 Calibration free method for measurement of the AC magnetization loss *Supercond. Sci. Technol.* **18** 592
- [36] Ekin J 2006 *Experimental Techniques for Low-Temperature Measurements: Cryostat Design, Material Properties and Superconductor Critical-current Testing* (Oxford : Oxford University Press)
- [37] Grilli F, Pardo E, Stenvall A, Nguyen D N, Yuan W and Gömöry F 2013 Computation of losses in HTS under the action of varying magnetic fields and currents *IEEE Trans. Appl. Supercond.* **24** 78–110
- [38] Ainslie M D, Yuan W, Hong Z, Pei R, Flack T J and Coombs T A 2010 Modeling and electrical measurement of transport AC loss in HTS-based superconducting coils for electric machines *IEEE Trans. Appl. Supercond.* **21** 3265–8
- [39] Wang M, Zhang M, Song M, Li Z, Dong F, Hong Z and Jin Z 2018 An effective way to reduce AC loss of second-generation high temperature superconductors *Supercond. Sci. Technol.* **32** 01LT
- [40] Grilli F and Kario A 2016 How filaments can reduce AC losses in HTS coated conductors: a review *Supercond. Sci. Technol.* **29** 083002